Ongoing development of applications of the Cone Penetration Test in interpretation and design

Barry M. Lehane[1]

[1]*Department of Civil Engineering*
The University of Western Australia, Perth, WA, Australia
Barry.Lehane@uwa.edu.au

ABSTRACT

This paper presents recent research on the application of the cone penetration test to site characterisation and foundation design. Aspects considered related to characterisation include the interpretation of relative density in granular soils, the derivation of the penetration-velocity characteristic, corrections for shallow penetration and scale effects in laboratory experiments and the influence of particle size on penetration resistance. In relation to foundation design, the paper outlines the nature of CPT-based correlations and describes the development of three types of such correlations for footings, axially loaded piles and laterally loaded piles.

Keywords: Cone penetration test; site characterisation; foundation design.

1. Introduction

The energy required to insert a probe into the ground reflects the strength and stiffness of the ground and this principle has been used for many years to assess the nature of the ground and to assist selection of suitable foundations. The Standard Penetration Test (SPT) standardized the input energy and probe geometry about a hundred years ago (Rogers 2006) and this standardization greatly assisted the development of more generally applicable empirical correlations with geotechnical parameters. Such correlations are, however, acknowledged to be highly approximate due to the sensitivity to drilling disturbance of SPT data as well as to shortcomings of the theoretical framework underpinning the correlations.

The Cone Penetration Test (CPT) has now replaced the SPT as the most popular in-situ test in many parts of the world. The CPT is, for most soils, a more convenient and cost-effective testing method, and provides a continuous and accurate digital profile of the ground resistance, free from drilling or operator dependent errors. With the ongoing development and improvement of CPT soil behaviour type (SBT) charts (e.g. Robertson 2009), practitioners can now have a high degree of confidence regarding the stratigraphy and soil types at any particular CPT location. In addition, direct relationships between a foundation response and the cone resistance (q_t) have continued to evolve and improve.

This paper provides an overview of some recent research by the author and co-workers on the interpretation of cone resistance profiles and on the use of CPT data to predict foundation response. In relation to profiling with the CPT, the paper describes improvements in techniques that deal with scale and shallow penetration effects and also discusses relationships between cone resistance and cone velocity in a range of soils and between cone resistance and relative density in granular deposits. The basis for recently published CPT-based design methods for foundation responses is then described and examples are provided that illustrate the applicability of these approaches for a range of foundation types. The sensitivity of these approaches to site variability is also discussed.

2. Simple interpretation of CPT

Before describing some recent developments related to the interpretation and use of the CPT, it is of interest to appreciate the factors, and their relative influence, on the magnitude of the recorded end resistance, q_t. These factors can be examined using the cavity expansion approximation for modelling cone penetration such as employed and verified by Yu & Mitchell (1998), Salgado et al. (1997), and others. The relative influence of factors controlling the drained cone resistance (q_{td}) was illustrated by Doan & Lehane (2020) who conducted regression analysis of the values of q_{td} predicted using the Yu & Carter (2002) cavity expansion solution in a drained, linear-elastic Mohr-Coulomb (MC) soil. The regression involved a wide range of initial mean effective stresses (p'_0), soil shear stiffness values (G), friction angles (φ') and dilation angles (ψ) and led to the following simple expression, which was found to predict the computed normalized cone resistance (q_{td}/p'_0) with a coefficient of variation of 0.2:

$$q_{td}/p'_0 = 3.6\,(G/p'_0)^{0.7}\tan(\phi' + \psi) \qquad (1)$$

Houlsby & Hitchmann (1988) demonstrate that the CPT end resistance in sand varies directly with the in-situ lateral effective stress (σ'_{h0}) and is relatively insensitive to the vertical effective stress (σ'_v). Doan & Lehane (2020) therefore re-configured Equation (1) assuming the

operational shear stiffness (G) varies with the soil's constrained modulus to show that the following equation could represent cone resistances observed in experiments in normally consolidated clay-sand mixtures (where v is the specific volume and λ is the compression index):

$$q_{td} \approx 6\,\sigma'_{h0}\,(v/\lambda)^{0.7}\tan(\phi' + \psi) \qquad (2)$$

A comparison of measured q_{td} values with those calculated using Equation 2 is shown on Figure 1. The dilation angles (ψ) used for each soil in the calculations were derived so that the shear strengths predicted using the linear elastic MC model corresponded to the measured strengths at 10% shear strain. Best-fit ψ values ranged from +10° for sand with 5% kaolin to -10° for sand with 25% kaolin.

Equation (2) evidently provides reasonable estimates for q_{td} over two orders of magnitude. Therefore, withstanding the limitations of the linear elastic Mohr Coulomb model, the equation captures the relative contribution of various factors to the *drained* CPT end resistance. For example, the expression indicates that q_{td} depends strongly on the dilative tendency of the soil surrounding the cone (approximately doubling as ψ increases from -5° to +10°) as well as on the inverse of the compression index (which typically varies by a factor of 10 or more between a sand and clay).

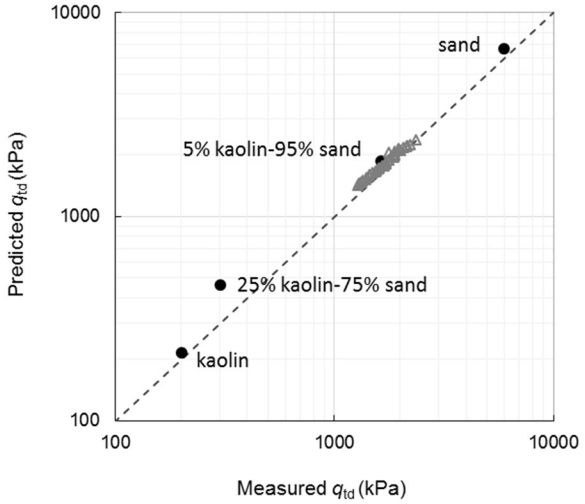

Figure 1. Measured cone resistances compared with those calculated using Equation (2)

Due to pore pressure generation during cone penetration in soils of low permeability, the CPT end resistance (q_t) in a standard cone test is usually lower than q_{td} in clays and silts. Equation (2) may then be more generally described as:

$$q_{td} \approx 6\,f_d\,\sigma'_{h0}\,(v/\lambda)^{0.7}\tan(\phi' + \psi); \quad f_d = q_t/q_{td} \qquad (3)$$

where f_d is a factor which falls from a value of unity for drained penetration to a minimum value of between 0.2 and 0.5 for undrained penetration (Kim *et al.* 2008, Jaeger *et al.* 2010 and Suzuki & Lehane 2015b); f_d usually increases with penetrometer velocity after undrained conditions are first reached due to viscous effects.

3. Drained penetration in granular soils

One of the most common applications of the CPT is the assessment of the relative density of a granular deposit. To assist in this regard, empirical relationships have been developed from laboratory CPTs conducted in reconstituted soils placed at a various relative densities (D_r) and consolidated to a range of stress levels. Proposed relationships are typically of the following format:

$$D_r = C_1 \ln[q_{c1N}/C_2] \qquad (4a)$$
$$q_{c1N} = [(q_c/p_a)/(\sigma'/p_a)^n] \qquad (4b)$$

where q_{c1N} = stress normalized cone resistance; C_1 and C_2 are empirical constants, p_a = atmospheric pressure (100 kPa), n = stress level exponent (typically between 0.5 and 0.7) and σ' is either the vertical, lateral or mean effective stress at the level of the cone tip.

Correlations of the form of Equation (4) have been proposed by Lunne & Christoffersen (1983), Baldi et al. (1986), and many others. Tian & Lehane (2022) compared these correlations against new measurements made in multiple CPTs performed in a calibration chamber containing a normally consolidated, uniformly graded, fine to medium, silica sand. The best-fit relationship obtained to the new data set was:

$$D_r = 0.37 \ln[q_{c1N}/21]$$
$$\text{with} \quad q_{c1N} = [(q_c/p_a)/(\sigma'_v/p_a)^{0.7}] \qquad (5)$$

As seen on Figure 2, this relationship is closely matched by those proposed for typical silica sands by Lunne & Christoffersen (1983) and Baldi et al. (1986). It might therefore be concluded that any of the three relationships will enable a reasonable estimate of D_r from q_c to be obtained in normally consolidated sand.

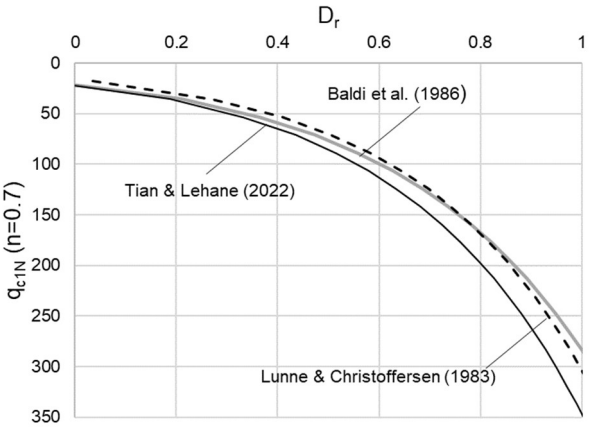

Figure 2. Correlations between normalised cone resistance and relative density in normally consolidated sand

Tian & Lehane (2024b,c) extended the investigation of Liu & Lehane (2012) to quantify the effect of particle shape and mineralogy on cone resistance. The combined set of results at one typical relative density (D_r=0.65) and

stress level (σ'_v =75 kPa, σ'_h =37 kPa) in normally consolidated granular deposits is shown on Figure 3. A marked tendency for q_c (and hence q_{c1N}) to increase with the soil's friction angle is evident despite no inclusion in Equation (5) of a dependence on friction angle. The trend indicated on Figure 3 is consistent with the simplified expression developed from cavity expansion theory (Equation 2) confirming that expressions such as Equation (5) should, at best, be considered as very approximate relationships with a high margin for error.

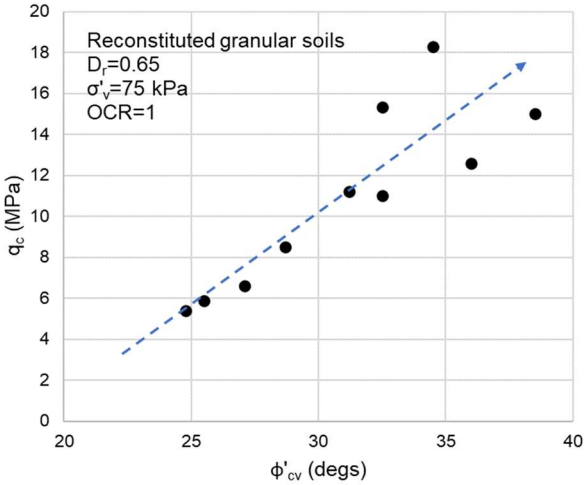

Figure 3. Measured cone resistance in various normally consolidated sands with D_r =0.65 and σ'_v =75 kPa

Tian & Lehane (2024b) show that the relationship between q_{c1N} and D_r could be made more generally applicable if the dependence on the sand's friction angle is incorporated. The stress levels beneath a cone are high and hence the operational friction angle during penetration is likely to be closer to the constant volume friction angle (φ'_{cv}) than the peak angle (φ'_p). This characteristic coupled with the fact that φ'_{cv} is independent of D_r indicates that a more practical relationship between q_{c1N} and D_r would involve φ'_{cv}. The value of φ'_{cv} varies with the mineralogy, particle shape and grading and can be assessed from measurement of the angle response of the dry sand or from a simple assessment of its angularity and mineralogy.

The following best fit relationship was obtained by Tian & Lehane (2024c) from results obtained in about 60 CPTs conducted in calibration chambers in 10 different sands (where $\mu_{cv} = \tan \varphi'_{cv}$):

$$D_r = 1.3 \exp(-2\mu_{cv}) \ln q_{c1N}/21 \qquad D_r > 0.3 \qquad (6)$$

This equation has the same format as Equation (5) but replaces the 0.37 multiplier with a friction angle dependent multiplier. The coefficient of variation of the ratio of measured D_r values to those calculated using Equation (6) is approximately 0.1 and significantly less than that of Equation 5. Tian & Lehane (2024c) also found that, in contrast to the interpretation made by Jamiolkowski et al. (2003), effects of compressibility in their database were not significant (although they may be masked by the higher friction angles of the more compressible carbonate sands). More data are required to confirm this trend. In addition, it is noted that Equation (6) has reduced reliability in very loose sands ($D_r < 0.3$) for which the stress exponent, *n*, was noted to be closer to unity in looser, more rounded sands.

While Equation (6) works well for normally consolidated unaged sands in calibration chambers, it is well known that the D_r *vs* q_c relationship depends on the age of the deposit and the in-situ lateral stress (or OCR); see Houlsby & Hitchman (1988), Tian & Lehane (2022). The following modified form of Equation (6) is therefore tentatively proposed for natural aged sands (with D_r >0.3)

$$D_r = 1.3 \exp(-2\mu_{cv}) \ln [\xi\, q_c/(34\, p_a^{0.3} \sigma'^{0.7}_{ho})] \qquad (7)$$

In this equation, the in-situ lateral stress (σ'_{ho}) is used in placed of the vertical effective stress and was derived assuming $\sigma'_{ho} = 0.5\sigma'_v$ in normally consolidated sand. ξ is an ageing factor which Lehane et al. (2004) showed was approximately 0.66 in a Quaternary dune sand deposit.

CPTs are often conducted in advance of deep excavations required for basement construction. Equation (7) can be used, combined with these initial CPTs, to estimate q_c values corresponding to those measured in CPTs performed at basement level for use in pile design. Values of q_c following scour around offshore/marine piles may also be estimated using Equation (7).

4. Dependence of penetration resistance on cone velocity

Standard CPTs are performed at a penetration rate of 20 mm/s. Pore pressure measurements made at the cone shoulder indicate that this rate generally leads to fully drained conditions in sand and fully undrained conditions in clay. However partial drainage of excess pore pressures generated during penetration in intermediate soils complicates interpretation of soil strength and stiffness in these materials.

Research on the rate dependency of penetrometer resistance indicates that the cone resistance is generally less than the fully drained value ($q_{t,d}$) when pore pressures are induced during penetration. With increasing cone velocity (v_c) and less time for dissipation of excess pore pressures, the resistance continues to drop and finally reaches the undrained value ($q_{t,u}$). Cone resistances increase modestly with increasing v_c during undrained penetration due to growing effects of soil viscosity. Finnie & Randolph (1994) were first to propose that cone resistance in the partially drained range is a function of the following normalised velocity term, V_v, which combines the soil's consolidation characteristics and the consolidation drainage path length, which varies with the penetrometer diameter (d_c):

$$V_v = v_c\, d_c/c_v \qquad (8)$$

where c_v is the vertical coefficient of consolidation determined in an oedometer or Rowe cell test. The use of Equation (8) in practice is hampered by the need to measure c_v in a laboratory test. In addition, the horizontal coefficient of consolidation, as measured in a piezocone penetration test (c_h), is considered more representative of

the operational coefficient during cone penetration. Suzuki (2014) confirmed that normalised velocity term, $V_{h,,}$ defined as follows, unified variable rate penetrometer data for Bassendean clayey silt and Burswood clay for which c_h values differed by more than a factor of 10.

$$V_h = v_c\, d_c/c_h \qquad (9)$$

A thorough review of the rate dependency of penetrometer resistance as seen in field, pressure chamber and centrifuge tests is provided in Suzuki (2014). This review showed that, while the V_h values indicative of fully drained and fully undrained penetrometer response do not differ significantly, the resistance normalised by the drained resistance ($q_t/q_{t,d}$), at a given V_h value, is strongly related to the nature of the soil and, in particular, to its tendency for a contractive or dilative response in shear (as may be inferred from Equations 2 and 3). The range of responses observed is illustrated in Figure 4, which shows that for highly contractive/sensitive soils, the undrained resistance may be as little as 10% of the drained resistance. Conversely, in dense dilative sand, the undrained resistance can be higher than the drained resistance (e.g. Silva 2005).

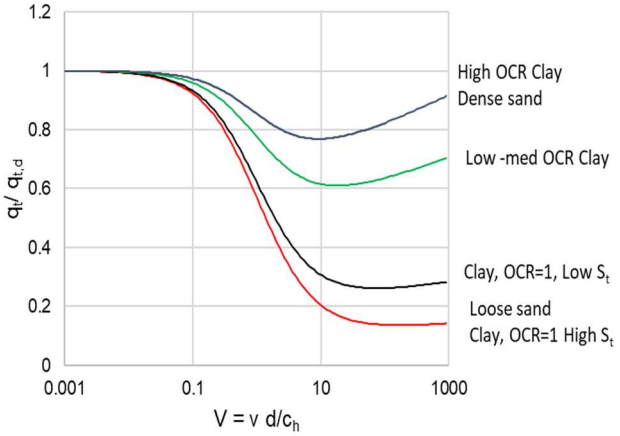

Figure 4. Typical variation of cone resistance (normalised by drained cone resistance) with normalised velocity in different soil types (based on Suzuki 2014)

Recent incidences of 'pile run' in offshore Taiwan and the UK highlight the importance of understanding the nature of the penetration-velocity characteristic for piling projects. In these examples, the drained soil strength was insufficient to carry the weight of the long (heavy) driven piles when they were pitched on the seabed. Consequently, the pile's downward velocity increased and, as it did, so did soil resistance (see Figure 4) leading to accelerating downward movement as the soil resistance dropped to that corresponding to undrained conditions (ignoring viscous effects). The 'pile run' ended when the undrained resistance of the soil was sufficient to carry the (submerged) pile weight.

While Figure 4 captures the essential features of the rate dependence of penetration resistance, determining the level of partial drainage in any given layer requires a separate calculation to determine V_h. The general trends indicated on Figure 4 are therefore recast using the time taken for 50% dissipation of excess pore pressure (t_{50}) as measured in a piezocone dissipation test using a standard 10cm^2 cone with v_c=20mm/s. The Teh & Houlsby (1991) solution for pore pressure dissipation at the cone shoulder was employed to relate c_h with t_{50} while limiting V_h values of 0.06 and 30 were presumed at the beginning and end of the partially-drained range. It so happens that value of t_{50}, expressed in seconds, calculated in this way is closely comparable to the value of V_h for a standard 10cm^2 cone with v_c = 20mm/s (and a soil rigidity index of about 100).

The general trends shown on Figure 4 are re-plotted on Figure 5 for cases where the ratio of undrained to drained resistance ($q_{t,u}/q_{t,d}$) is 0.6 (a typical value for a clay with low to moderate OCR) and 0.2 (typical of a sensitive soil with OCR=1). It is evident that the penetration resistance can be considerably less than the drained resistance in soils with very low t_{50} values (e.g. silts). For example, the cone resistance is only about half the drained resistance value in a sensitive soil with OCR=1 and a t_{50} value of 2 secs. Given this short duration, it is likely that the measured cone resistance in such a soil is presumed by designers to equal the fully drained resistance i.e. $q_{t,d}$ is underestimated significantly.

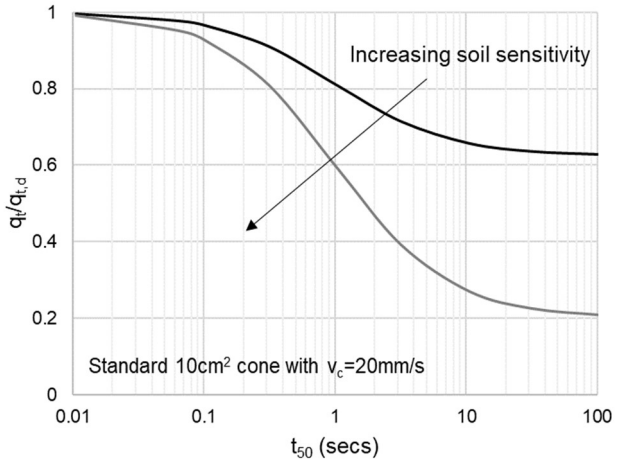

Figure 5. Penetration resistance variation with t_{50} measured in a piezocone dissipation test

Even though variable rate penetrometer tests have been advocated for many years, their use in practice is not widespread. It is suggested here that simply increasing the cone rate from the standard of 20mm/s to a non-standard, fast rate of 100mm/s over a short distance (350mm or 10 cone diameters) is easily achievable in practice and would greatly assist interpretation of the penetration resistance-velocity characteristic. This is because the curves shown on Figures 4 and 5 can be expressed as follows (noting, as discussed, $V_h \approx t_{50}$ (secs) and ignoring viscous effects):

$$q_t = q_{t,d} - \frac{(q_{t,d} - q_{t,u})t_{50}(s)}{1 + t_{50}(s)}$$

$$\approx q_{t,d} - \frac{(q_{t,d} - q_{t,u})V_h}{1 + V_h} \qquad (10)$$

The actual $q_t/q_{t,d}$ variation with V_h can be constructed knowing (i) q_t at 20mm/s, (ii) q_t at 100mm/s and (iii) the value of t_{50} determined from a dissipation test. For example, if the q_t value in a soil with a t_{50} value of 10 secs is 3 MPa and this cone resistance reduces to 2 MPa at a cone speed of 100mm/s, two simultaneous equations are obtained when substituting q_t of 3 MPa with V_h=10 and q_t= 2MPa with V_h=50 into Equation (10). The solution for this case is illustrated in Figure 6 which shows that the measured cone resistances are much closer to the undrained range and the drained cone resistance is about five times higher than q_t measured at 20mm/s.

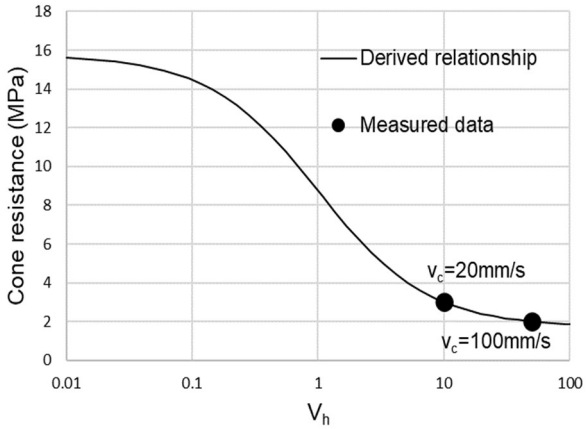

Figure 6. Example illustrating how the cone resistance-velocity relationship is derived from Equation (10)

5. Dependence of penetrometer resistance on diameter

The effect of diameter on penetration resistance is significant in the interpretation of laboratory-scale penetration experiments and in the assessment of soil properties of thin layers in the field from the CPT. The relationship between the end bearing of a displacement pile during installation and the cone resistance is also diameter dependent.

5.1 Centrifuge CPTs : Shallow penetration and stress gradient effects

A typical example of a cone resistance profile measured at two g-levels (40g and 100g) in a geotechnical centrifuge is shown on Figure 7 (Lehane et al 2023). This figure plots the variation of q_c with vertical effective stress (σ'_v) measured using a 7mm diameter cone in sand with a relative density (D_r) of 0.8. It is apparent that there is not a unique relationship between q_c and σ'_v, despite the sand having the same D_r value. In addition, for the test conducted at 100g, the rate of change of q_c with σ'_v tends to increase a little up to σ'_v =120 kPa and reduce slightly at greater stresses. These changes are small, however, and the overall variation of q_c with depth over the σ'_v range plotted can be approximated as a linear relationship for a particular g-level. While such linearity is commonly assumed in the assessment from q_c data of a centrifuge sample's relative density tests (e.g. Schneider & Lehane 2006), it is clearly inconsistent with the non-linear dependence of q_c on σ'_v inferred from calibration chamber tests (e.g. Jamiolkowski et al. 2003, Lunne & Christoffersen 1983).

Miniature CPTs conducted to up to a penetration of 400mm in the very deep centrifuge strong boxes at the Technical University of Denmark (DTU) revealed that the apparent linear dependence seen on Figure 7 arises because of shallow penetration effects, which vary with both the diameter of the centrifuge cone (d_c) and the g-level employed.

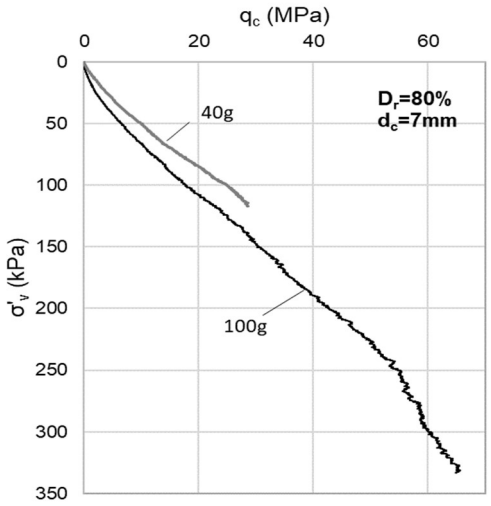

Figure 7. Cone resistance profiles measured in the centrifuge in dense sand with a 7mm diameter cone

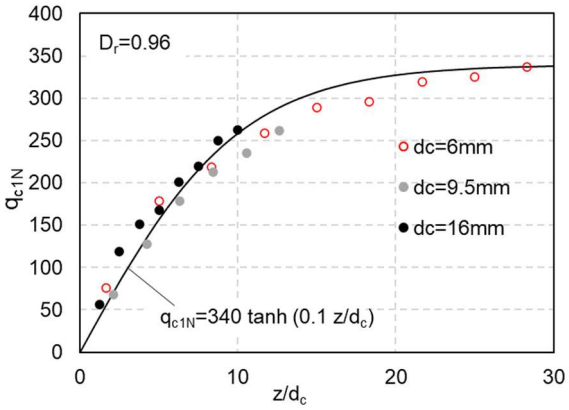

Figure 8. Cone resistance profiles measured in the centrifuge in dense sand with a 7mm diameter cone

Data re-plotted from centrifuge measurements of Xu (2007) obtained with three different diameter cones in a dense sand are presented on Figure 8, which plots normalised cone resistances, q_{c1N}, calculated using Equation (4b) with n=0.7 and $\sigma'=\sigma'_v$, against penetrometer depth normalised by the cone diameter (z/d_c). It is seen that the q_{c1N} values from the three cone diameters are unified and display the same variation with z/d_c, increasing to a steady state stress normalised resistance at a penetration of about $20d_c$.

The hyperbolic tangent equation provided on Figure 8 evidently provides a good representation of the data. Use of the same function is examined on Figure 9 for q_c *vs* σ'_v data recorded by a 11.3mm diameter cone in Leighton Buzzard sand (Lehane et al. 2023). The full data set is seen to be well represented at all penetrations and

stress levels. Further tests indicated that the steady state (maximum) values recorded at given D_r values and stress levels were in excellent agreement with corresponding q_c values recorded in calibration chamber tests (where σ'_v is constant). Lehane et al. (2023) re-examined a large database of centrifuge CPT data using the same approach which confirmed that that the strong stress level gradient in centrifuge tests combined with shallow penetration effects explain the apparent inconsistencies between centrifuge and calibration chamber data.

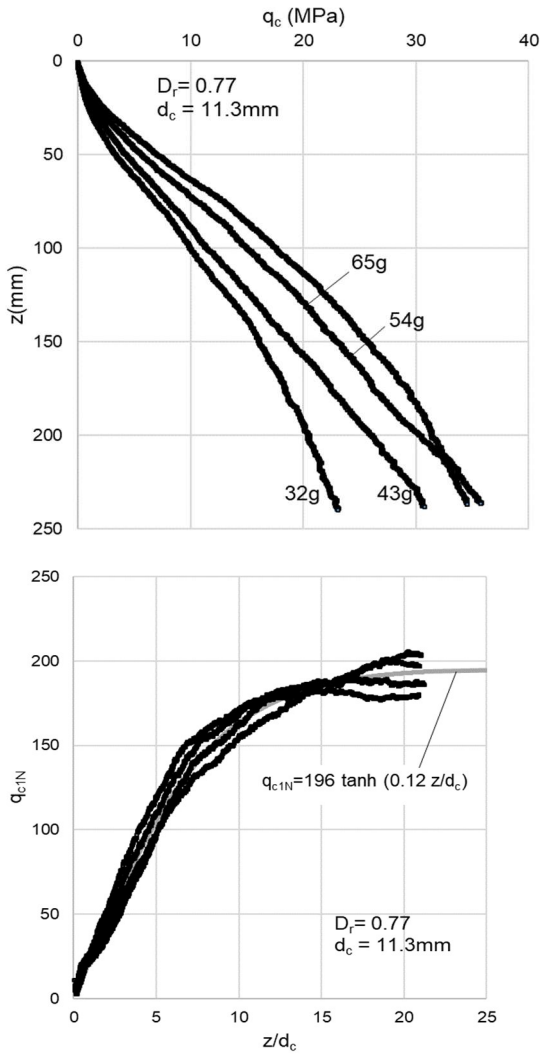

Figure 9. (a) cone resistance profiles measured at four g-levels in sand with Dr=0.77 and cone diameter, d_c =11.3mm, (b) data represented as variation of q_{c1N} with normalised depth (z/d_c)

The following best-fit expression was obtained by Lehane et al. (2022) for the silica sand database of centrifuge CPTs:

$$q_{c1N} = \frac{\left(\frac{q_c}{p_a}\right)\left(\frac{p_a}{\sigma'_v}\right)^n}{tanh\left(\frac{az}{d_c}\right)} \qquad (11)$$

where a = 0.66 exp (-2.5 D_r)

Relationships between cone resistance and foundation performance in centrifuge tests have not, in the past, been pursued because the trends indicated by the data were inconsistent with those seen in full scale tests e.g. Pucker et al. (2013) and Govoni et al. (2010). This is largely because of the lack of recognition of the scale effects embodied in Equation (11). More recently, however, a number of studies have re-assessed such relationships with scale effects incorporated. For example, Liu & Lehane (2021) demonstrate that the same relationship between bearing pressure, normalised displacement and cone resistance is achieved for centrifuge and full-scale footings using scale corrected q_c values. Similarly, Bittar et al. (2023) showed that the CPT-based empirical relationship established from field tests for the capacity of helical piles was also valid for the centrifuge-scale helical piles tested by Cerfontaine et al. (2021) when the CPT data was corrected for shallow penetration effects.

5.2 End bearing resistance of displacement piles

The end bearing of a displacement pile during installation can be expected to be similar to that of a cone penetrometer with the same diameter. Therefore, as the diameter of a pile is at least one order of magnitude larger than a cone, the zone of influence around the pile tip is significantly greater than around a cone. This diameter effect can be readily appreciated using the simple formulation developed by Tian & Lehane (2024a) from a range of penetrometer tests conducted in controlled experiments involving two discrete soil layers. The formulation is used in Figure 10 to deduce the end bearing resistance during driving of a 600mm diameter pile from the CPT data recorded at a site in East London, UK. It is evident that the estimated pile end bearing in the sand layer below 12m is influenced by the proximity of the overlying soft clay and only approaches that of the CPT after a penetration of about 8m into the sand.

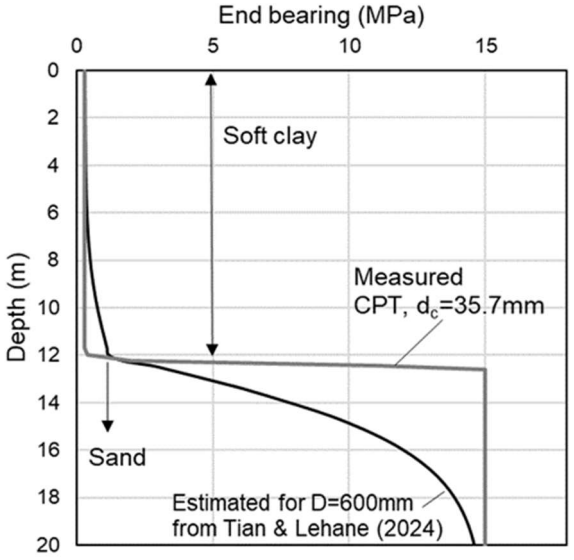

Figure 10 Penetration resistance for a standard cone compared with estimated resistance for a 600mm closed-ended pile

Closed-ended, bottom-driven, 600mm diameter steel tubes were installed to a depth of 14 m (2m penetration into sand) for a jetty structure at this London site in the 1980s. However dynamic testing showed that the end bearing mobilized was significantly lower than anticipated/required. A decision was made by the contractor to re-drive all piles for the project to a minimum penetration of 4m into the sand, which dynamic tests indicated was sufficient to satisfy the design requirements. Although full knowledge at the time of why this additional penetration was required was not known, it is clear from Figure 10 that the initial pile design had under-estimated the zone of influence of the piles and the required 'development length' into the dense sand layer.

5.3 Influence of layering on cone resistance

The influence of adjacent soil layers on the penetrometer resistance can be more generally calculated using the Boulanger & DeJong (2018) method (B&D method), which determines the penetration resistance of an infinitely small penetrometer, referred to as the true cone resistance (q_c^t). This is achieved using an inverse filtering approach commonly used in image and signal processing and is based on the premise that the cone resistance measured at any particular depth is influenced by all of the soils in the vicinity of the tip, with greater weighting being applied to soils closest to the tip. Tian & Lehane (2024a) introduced modifications to the B&D weighting formulations based on a series of experimental observations. Typical predictions using the 'modified B&D formulations' are shown on Figure 11 for a model cone test in a multi-layered stratigraphy. The method was used to predict actual (normalized) cone resistances using the 'true' resistances determined from the as-placed relative densities and undrained strengths and evidently works well (and displays better matching to measurements than the original B&D weighting coefficients). The stark difference between the true and measured normalized resistances shown on this plot highlights the very significant scale effects that arise in laboratory test set-ups.

5.4 Size effect: influence of large particles

There is often uncertainty regarding the assessment of cone resistance in gravels because of their relatively large particle size (compared with the cone size) leads to considerable fluctuations in measurements. Tian & Lehane (2024c) investigated the effect of the ratio of mean particle size (d_{50}) to cone diameter (d_c) in calibration chambers using cones with d_c= 6mm and 16mm in uniformly graded glass ballotini with d_{50} =0.9mm; these parameters correspond to d_{50}/d_c values of about 6.5 and 18. Bolton et al. (1999) recommend a minimum d_{50}/d_c ratio of 20 to ensure no size effect.

Results with the two cone sizes in a medium dense deposit at a vertical effective stress of 50 kPa are shown on Figure 12a. As expected, it is seen that the fluctuations in q_c for the smaller diameter cone are very high, with variations about the mean being about 50% of the actual mean value. A similar level of variation was seen in dense samples.

Figure 12b plots the same data but using running average values measured over a distance of 5mm. It is seen that, apart from deviations near the upper part of the sample (which may be partly due to shallow penetration effects), there is very close agreement between the average profiles recorded by the two cone diameters. This result indicates that averaged cone resistances in gravels, where significant fluctuations occur, are representative of a q_c profile corrected for size effects.

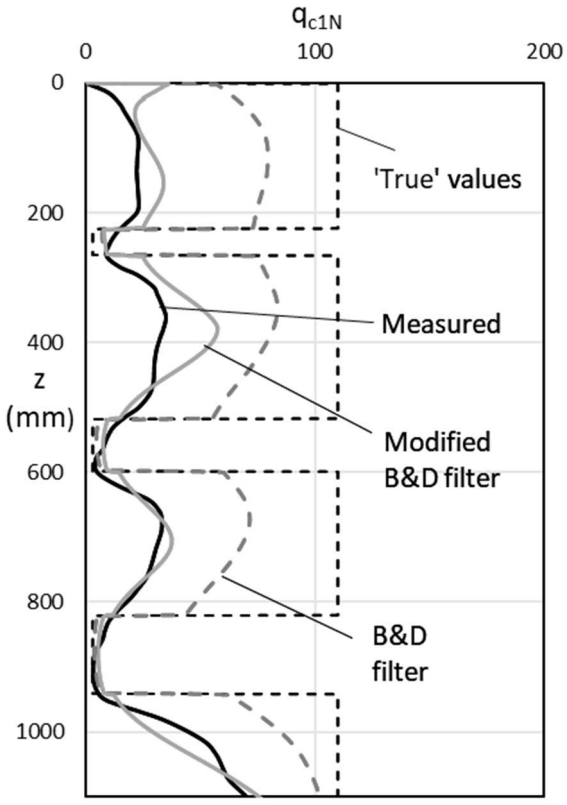

Figure 11 Measured and predicted cone resistance normalised cone resistance profiles in a multi-layered stratigraphy

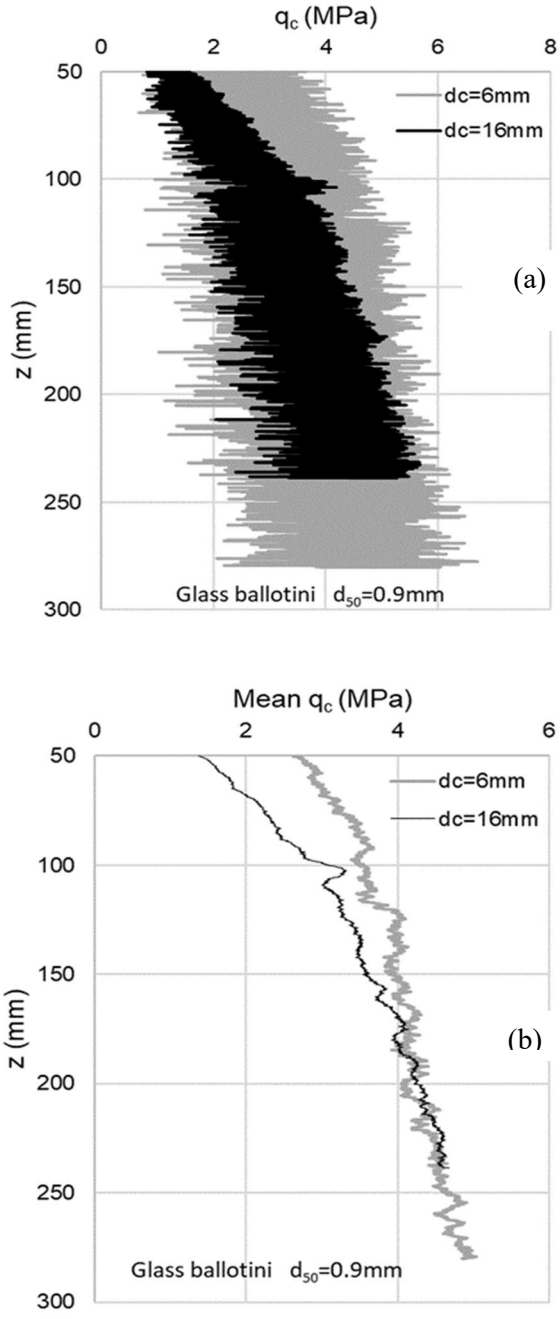

Figure 12 Cone resistance profiles measured in glass ballotini with two cone diameters (a) measured resistance profiles and (b) averaged resistance profiles

6. CPT-based correlations for foundations

CPT-based correlations employed for prediction of the capacity and stiffness of deep foundations have been shown for many years to perform better than other in-situ test based methods (e.g. Briaud & Tucker 1988). The relative success of these earlier correlations can be attributed to the more repeatable and continuous data obtained in a CPT (compared, for example, to the discrete and driller dependent blowcounts measured in Standard Penetration Tests). More recently, a marked improvement in method reliability has been observed when correlations incorporate the physical basis for inclusion of cone resistance in the formulations and combine this with other factors which are not related to the cone resistance but also affect the foundation response. The justification for use of the cone resistance in various correlations for foundations is provided in Table 1, which also lists other important geometrical features and soil properties that need to be incorporated in the correlations.

Table 1. Nature of CPT correlations

Foundation	Basis of CPT-based correlation	Factors incorporated in CPT-based method
Shallow footing in sand and clay	Deformation mode before formation of bearing capacity mechanism is comparable to cavity expansion	Normalised settlement
Shaft friction on driven pile in sand	Stationary horizontal effective stress acting on shaft is directly proportional to the qc value	Normalised distance from pile tip (h/D) Displacement induced during installation (open vs closed ended piles) Interface friction angle. Loading direction, age
End bearing of pile driven pile	Mode of penetration of driven pile is comparable to penetrometer	Partial mobilsation of resistance (due to relatively small pile penetrations) Scale effects due to large diameter of pile
Shaft friction on driven pile in clay	Stationary horizontal total stress acting on shaft is varies directly with qt (but relationship depends on clay)	Stress changes post-installation as pore pressures dissipate and clay creeps Displacement induced during installation (open vs closed ended piles) Clay sensitivity, interface friction angle, age
Shaft friction of bored pile	In-situ lateral effective stress varies with qt	Soil type dependence Dilation contribution in sand
Helical pile	Loading at helix analagous to cavity expansion	Direction of loading Shaft friction (usually small) Number of helices
Laterally loaded pile in sand	Numerical calibration of lateral pressure with qt	Wedge type failures at shallow depth Pile diameter and shape, stress level Pile rigidity
Laterally loaded pile in clay	Analytical solutions showing ult. pressure vary with su and hence $_{qt}$	Wedge type failures at shallow depth Pile diameter and shape, stress level Pile rigidity

Table 2. Unified method for capacity prediction of axial capacity of driven piles (Lehane et al. 2022)

$Q_{shaft} = \pi D \int_0^L \tau_f \, dz$

$Q_{base} = q_{b0.1} (\pi D^2/4)$

Capacity estimate for piles for flexible piles in strain-softening clays requires load-transfer analysis using load transfer curves given in API (2011)

Sands: Zone 6 of SBT chart (I_c< 2.1)

$\tau_f = f_L (\sigma'_{rc} + \Delta\sigma'_{rd}) \tan 29^o$

$q_{b0.1} = [0.12 + 0.38A_{re}]q_p$; for plugged base (expected when L/D>5)

$q_{b0.1} = A_{re} q_p$; for unplugged base

$\sigma'_{rc} = (q_c/44) A_{re}^{0.3} \left[\text{Max}[1, h/D]\right]^{-0.4}$

$\Delta\sigma'_{rd} = (q_c/10) (q_c/\sigma'_v)^{-0.33} (d_{CPT}/D)$

$A_{re} = 1 - PLR (D_i/D)^2$

$PLR \simeq \tanh \left[0.3 (D_i/d_{CPT})^{0.5}\right]$

f_L= 0.75 in tension, 1.0 in compression

q_p can be taken as the average q_c within a zone 1.5D above and below the pile tip or determined using the procedure described Boulanger & De Jong (12018) and Bittar et al. (2020)

Clays: Zones 1,2,3 & 4 of SBT chart

$\tau_f = 0.07 F_{st} q_t \left[\text{Max}[1, h/D^*]\right]^{-0.25}$

$q_{b0.1} = [0.2 + 0.6A_{re}]q_p$

F_{st} =1 for clays with I_{z1}>0, in Zones 2, 3 and 4 on the SBT Chart ($I_c \geq 2.6$)

F_{st} =0.5±0.2 clays with I_{z1}<0, in Zone 1 on the SBT Chart

$D^* = (D^2 - D_i^2)^{0.5}$ for an open-ended pile and D^*=D for a closed-ended pile

$I_{z1} = Q_{tn} - 12exp^{(-1.4F_r)}$

q_p =average q_t value in zone between the pile tip and 1D below the pile tip (closed-ended/ plugged pile) or average q_t to a depth of 20t below the pile tip (large diameter, unplugged pile)

Silts: Zone 5 of the SBT chart (2.1< I_c <2.6)

Apply equations as for Zone 6 using corrected q_c value determined as:

$q_c = [3.93 I_c^2 - 14.78 I_c + 14.78] q_t$

Table 3. Additional CPT correlations for foundations

Pad footings

$q = 0.45\, q_{t,avg} \tanh\left[6\left(\frac{s}{B}\right)^{0.5}\right]$ immediate settlement in clay

$$\frac{s}{B} = \left(\frac{q}{q_{c,avg}}\right)^2 \left[3 + 70\, c\, log_{10}\left(\frac{t(days)}{0.05}\right)\right]$$ long term in sand

Bored piles (drilled shafts), Doan & Lehane (2021)

$$\frac{\tau_f}{p_a} = 0.008\left(\frac{f_t}{f_c}\right)(I_c)^{1.6}\left(\frac{q_t}{p_a}\right)^{0.8} \quad \left(\frac{f_t}{f_c}\right) = 0.8$$ for tension loading in sand (and is unity otherwise)

$q_{b0.1} = 0.11\, I_c\, q_t \;\; 1.5 \leq I_c \leq 3.6$

Laterally loaded piles, *Suryasentana & Lehane (2016) and Truong & Lehane (2018)*

$$P = P_u\left[1 - exp\left(-8.9\left(\frac{y}{D_e}\right)\left(\frac{\sigma_v - u_g}{\sigma'_v}\right)^{0.5}\left(\frac{z}{D_e}\right)^{-1.25}\right)\right] \;;\; y/D_e \geq 0.01$$ (sand)

$$P = P_u \tanh\left[5.45\left(\frac{y}{B}\right)^{0.52}\right]$$ (clay)

$$P_u = 2.4\,\sigma'_v\left(\frac{q_c}{\sigma'_v}\right)^{0.67}\left(\frac{z}{D_e}\right)^{0.75} \leq q_c$$ (sand)

$$P_u = 0.9\, q_{t,net}\left[1 - 0.75e^{-0.6z/B}\right]S_p$$

S_p = *1.0 for circle & 1.25 for square section* (clay)

Load-displacement response of driven piles, Lehane et al. (2020), Lehane et al. (2022)

$$\frac{\tau}{\tau_f} = 2\frac{w}{w_f}\left[1 - \frac{w}{2w_f}\right]$$

$$\frac{w_b}{D} = 0.01\left[\frac{q_b/q_{b0.1}}{1 - 0.9\,(q_b/q_{b0.1})}\right]$$

In sand : $\frac{w_f}{D} = \frac{{q_c}^{0.5}{\sigma'}_v^{0.25}}{Ap_a^{0.75}}$ $A = 1250$ *in compression,* $A = 625$ *in tension*

In clay : $\frac{w_f}{D} = 0.01$

Axial response of helical piles in sand (Bittar et al. 2023)

$$Q = \left(\frac{\pi D_h^2}{4}\right)\left(k\, q_{c,avg}\left(\frac{\delta}{D_h}\right)^{0.6}\right) + Q_{shaft};\;\; \delta > 0.01d$$

k=0.6 in tension and 0.8 in compression; $Q_{shaft} = (q_{cs}/230)\, A_{shaft}$

$$T\,(kNm) = \left[(q_{cs}/230)A_{shaft} + 0.15 q_{c,avg}(\pi\, D_{hi}^2/4)\right] \times 0.4d(m)^{0.92}$$

A summary of correlations of this nature that have been proposed in various publications by the author are provided in Tables 2 and 3. This paper describes the basis and evolution of three of these correlations, each of which employs a different approach. The examples selected consider the (a) the load-displacement response of pad footings, (b) shaft friction of driven piles and (c) lateral response of piles in sand.

6.1. Load-displacement response of pad footings

6.1.1. Shallow Footings on sand

The bearing capacity of a shallow foundation on sand is still commonly calculated using traditional bearing capacity formulae, where the calculation requires determination of N_q and N_γ bearing capacity factors from an assessed friction angle. There is, however, limited evidence of full-scale shallow foundations in sand experiencing the classical bearing capacity failure implicit in the bearing capacity formulae. Lehane (2012) present data from 47 field tests in sand where the footings were loaded to a bearing stress sufficient to induce a settlement to width ratio (s/B) of 0.1. Although foundations would ordinarily be considered at the ultimate limit state at this s/B ratio, the mode of deformation of the footings at that stage displayed no indication of shear/rotational failure. Lehane (2012) showed that the measured bearing pressures at s/B=0.1, $q_{0.1}$, were not proportional to ultimate values calculated from the bearing capacity formulae. Therefore, aside from difficulties in selecting an appropriate operational friction angle for sands, values of $q_{0.1}$ cannot be reliably estimated using the traditional bearing capacity formula.

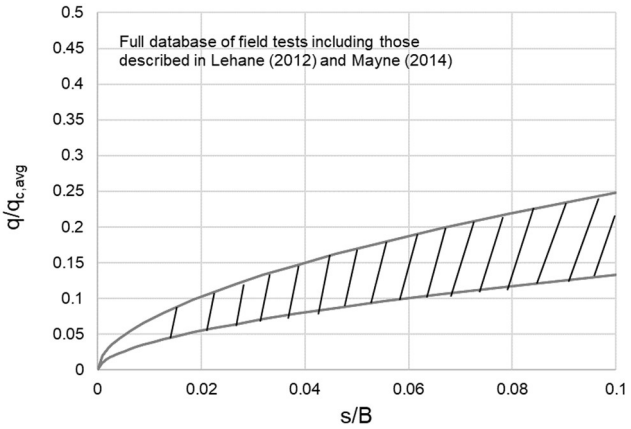

Figure 13 Normalised bearing pressure variation with normalised short-term settlement for footings on sand.

Numerical analyses by Bagbag *et al.* (2019), and others, confirm observations made through image analyses of centrifuge-scale embedded footings on sand (Sreng et al. 2005) that ground displacements emanate outwards from the centre of a footing at s/B ≤ 0.1 and that conditions are comparable to the expansion of a spherical cavity. Yu & Mitchell (1998) , and others, have shown that the CPT end resistance can also be well predicted using cavity expansion theory and hence a direct correlation between bearing stress on a footing and q_c value can be expected.

Available experimental data compiled by Lehane (2012) and Mayne (2014) confirm the strong correlation in sands between footing bearing pressure (q) and the average cone resistance within the zone of influence of the foundation ($q_{c,avg}$). Briaud & Gibbens (1999), Lehane et al. (2009) and others also show that the load-displacement response for different footings can be unified by normalising the settlement (s_i) by the foundation width (B); this s/B ratio is analogous to the cavity strain associated with cavity expansion. The envelope of results obtained from in excess of 70 tests on shallow footings founded on a wide range of sand types is presented on Figure 13 and can be represented by:

$$\frac{q}{q_{c,avg}} = (0.7 \pm 0.2)\left(\frac{s_i}{B}\right)^{0.55} \qquad (12)$$

Equation (12) indicates that the ultimate capacity of a footing, defined at $s_i/B=0.1$, is typically between (0.18 ± 0.04) $q_{c,avg}$ and about $0.05q_{c,avg}$ at a typical footing displacement at working load of 0.01B. Equation (12) can be used to determine the short term settlement (s_i) as it represents responses measured in load tests that typically took less than a couple of hours to complete.

Liu et al. (2022) expanded the investigation of creep settlements of footings on sand and confirm that the normalised creep settlement, s_c/B, can be expressed by the following expression when the bearing stress is less than about 50% of $q_{0.1}$ i.e. a factor of safety of about 2:

$$\frac{s_c}{B} = c\left(\frac{q}{q_{0.1}}\right)^2 ln\left(\frac{t}{t_{ref}}\right) \qquad (13)$$

where t_{ref} is a reference time that was assigned a value of 0.02 days to suit compilation of the available footing creep data. The creep parameter, *c*, was found to vary between 0.003 and 0.02 and site-specific measurements were recommended.

If the exponent in Equation (12) is reduced to 0.5, the mean multiplier of 0.7 needs to be adjusted to a value of 0.58 to represent the same approximate mean trend line. This adjustment combined with Equation (13) leads to the following simple CPT-based expression for the mean expected footing settlement at any time, t, after loading:

$$\frac{s}{B} = \left(\frac{q}{q_{c,avg}}\right)^2 \left[3 + 70\, c\, log_{10}\left(\frac{t(days)}{0.05}\right)\right] \qquad (14)$$

An illustration of predictions obtained using Equation (14) is provided in Figure 14, which shows the impact of time and the creep coefficient (c) on the normalised settlements at typical operational levels of footing settlement i.e. s/B between about 1 and 2%. It is seen that creep under static loading can be very significant for sands with a high *c* value of 0.02 (as shown by the dune

sands at Shenton Park and Ledge Point in Western Australia) but relatively modest in sands such as that tested by Briaud & Gibbens (1999) which indicated a *c* value of 0.003. Assessment of an allowable bearing pressure (typically requested by structural engineers) is therefore dependent on the sand's creep characteristics as well as on the expected loading history.

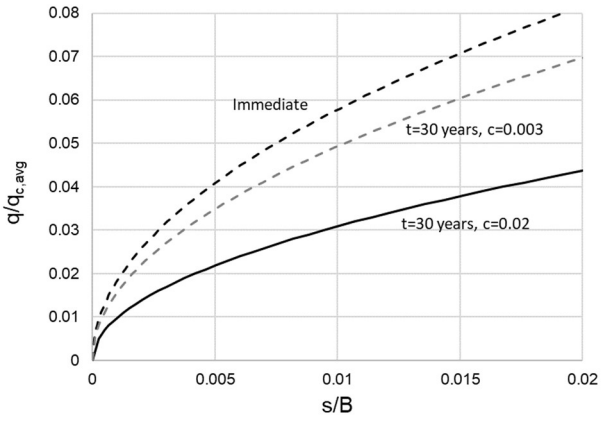

Figure 14 Normalised bearing pressure variation with normalised long-term settlement for footings on sand.

Equation (14) indicates that a bearing pressure of about $q_{c,avg}/25$ leads to a settlement of 1% of the footing width over the lifetime of an average structure for a typical mean *c* value of 0.01.

6.1.2. Shallow Footings on clay

Load displacement data compiled from undrained tests on shallow footings in four clays are presented on Figure 15 in a similar normalised format to that adopted for footings on sand in Figure 13. The result plotted for the Bangkok clay is the average trend obtained in five separate footing tests. The formation levels of the footings in Belfast, Bothkennar, Bangkok and Haga were at depths of 1.6m, 0.8m, 1.5m and zero respectively. Three of the four clays (Belfast, Bothkennar and Bangkok clay) are lightly overconsolidated whereas the Haga clay is overconsolidated with a vane shear strength of ≈ 45 kPa. Full details of the case histories are provided in Brand *et al.* (1972), Jardine *et al.* (1995), Andersen & Stenhamer (1982) and Lehane (2003).

A classical rotational shear failure occurred at relatively low s/B values in the tests conducted in Bangkok, Haga and Belfast whereas a punching failure appeared to occur at Bothkennar, possibly due to partial drainage occurring in an upper thin siltier layer. The average net cone resistance beneath the footings ($q_{net,avg}$) is used in place of $q_{t,avg}$ to normalise bearing stress in Figure 15 as this is understood to vary more directly with undrained shear strength (s_u) . There is, however, scatter in the observed $q_{0.1}/q_{net,avg}$ values which vary from 0.45 to 0.62. This scatter is consistent with variability between clays, reported by Jardine et al (1995), Lehane (2003), and others, of the ratio of the average operational undrained shear strength (s_{uop}) to any single s_u measure. For example, the ratio of s_{uop} to the vane shear strength for the same database of footing tests varies between 0.5 and 0.8 (noting s_{uop} is the s_u value used in the standard bearing capacity equation that gives a capacity equal to the measured capacity).

The best-fit mean trend line to data on Figure 15 is:

$$q = 0.55\, q_{net,avg} \tanh\left[6\left(\frac{s_i}{B}\right)^{0.5}\right] \qquad (15)$$

This equation provides a good fit to the observations up to s_i/B of about 0.02 when conditions are analogous to cavity expansion. Equation (15) can therefore be employed to obtain an estimate of immediate settlement at typical working loads. Deviations between the responses in different clays become evident at larger displacements when strength mobilisation extends beyond the zone below the footings and the shear failure mechanism develops.

It is also of interest to note the difference shown on Figure 15 between the variations of normalised bearing stress with s/B in clays and sands. Much of the difference is consistent with the higher cone resistances developed under drained conditions (e.g. Figure 4).

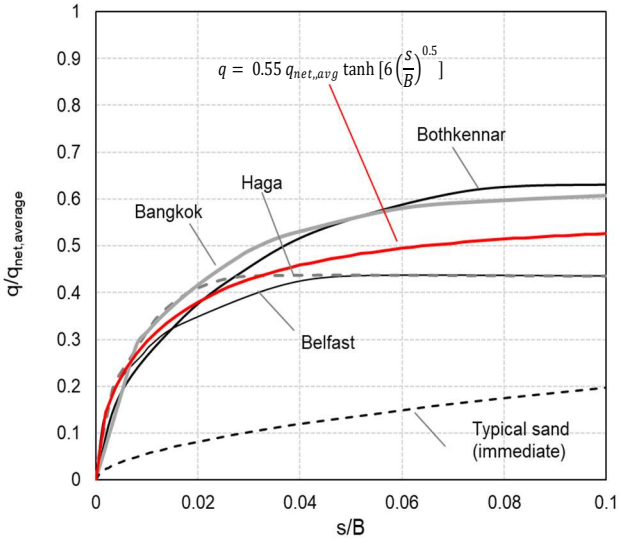

Figure 15 Normalised bearing pressure variation with normalised short-term settlement for footings on clay.

6.2. Shaft capacity of driven piles

The basis for a relationship between the ultimate shaft friction on a displacement pile and cone resistance emerged from experiments that employed piles equipped with radial stress sensors. These experiments indicated that there was a proportional relationship between the cone resistance and the radial stress acting on a pile in any given soil horizon during its installation. Two examples illustrating this dependence for piles in sand and clay are presented in Figure 16.

6.2.1. Piles in sand

The stationary radial effective stress (σ'_{rc}) profiles recorded by three sensors mounted on a pile in sand are shown on Figure 16a and seen to mirror the q_c profile. It is also evident that stress sensors located further from the pile tip in the same soil horizon (i.e. larger *h* values)

register lower radial stresses. These observations indicate that:

$$\sigma'_{rc} = f(q_c, h) \quad (16)$$

Further research with instrumented piles in sand showed that:

- Radial stresses increase (by an amount = $\Delta\sigma'_{rd}$) during pile loading due to constrained dilation.
- Effects of cavity contraction of sand at the pile shaft during the (cyclic) installation process, as well as other effects, are such that σ'_{rc} varies more uniquely with h/D than h.
- The magnitudes of the radial stresses vary with the degree of soil displacement imposed during installation (captured by a term referred to as the effective area ratio, A_{re})
- The interface friction angle (δ) between rough steel and sand is typically about 29° for all fine and medium grained sands (due to effects of sand crushing beneath the pile tip).
- Radial effective stresses do not vary significantly from those recorded during installation but values of $\Delta\sigma'_{rd}$ increase with time after installation.

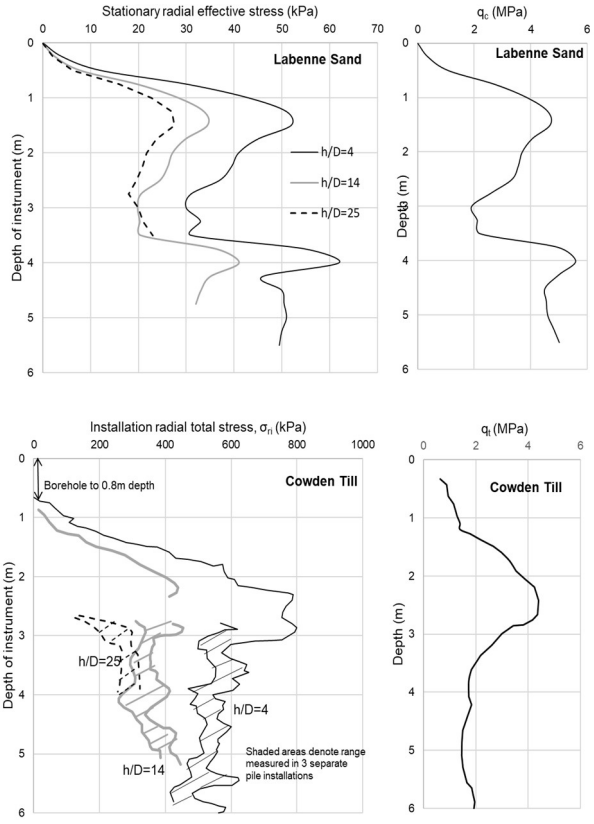

Figure 16 A comparison of radial stresses recorded during displacement pile installation and the cone resistance in sand and clay till.

These observations are incorporated in the calibration of a design method using a database comprising 70 high quality pile load tests data and lead to the formulations given in Table 2. These formulations relate to a set-up time of about 10 days and will underestimate capacities at longer ageing periods.

6.2.2. Piles in clay

The radial total stresses (and not the effective stresses) for piles in clay are seen on Figure 16b to vary with the cone resistance (q_t) and also vary with the distance from the pile tip (h) i.e.

$$\sigma_r \approx (\sigma_r - u_0) = f(q_t, h) \quad (17)$$

where u_0 is the ambient (hydrostatic) water pressure. After pile installation, in a process referred to as equalisation, radial total stresses generally reduce while excess pore pressures dissipate. These effects combine to lead to increasing radial effective stresses until consolidation is completed (when $\sigma'_r = \sigma'_{rc}$). The radial stresses during installation, equalisation and subsequent load testing stages in the life of a displacement pile can be described by the following stress coefficients:

$$S_i = (\sigma_{ri} - u_0)/q_t = f(h/D) \text{ or } f(h/D^*) \quad (18)$$

$$S_c = (\sigma_{rc} - u_0)/q_t = \sigma'_{rc}/q_t \quad (19)$$

$$f_L = \sigma'_{rf}/\sigma'_{rc} \quad (20)$$

Values of S_i observed in instrumented pile tests vary with h/D for closed-ended piles and vary approximately with h/D* for open-ended piles (where D* is defined in Table 2). However, the observed variations of S_i with h/D or h/D* depend strongly on the type of clay. The equalisation coefficient, S_c, ranges between about 0.3 and 0.9 while the load factor, f_L, defining the ratio of the radial effective stress at peak friction (σ'_{rf}) to σ'_{rc} is typically about 0.9 ±0.1.

Jardine et al. (2005), and many others, have confirmed the validity of Coulomb's friction law at the loading rates adopted in typical static load tests. Assuming Coulomb's friction law, Equations (17) to (20) then lead to the following expression for shaft friction (τ_f), which gives τ_f as a direct function of the corrected cone resistance q_t, the three stress coefficients and the interface friction angle (δ):

$$\tau_f = \sigma'_{rf} \tan\delta = q_t S_i (S_c/S_i) f_L \tan\delta \quad (21)$$

Equation (21) forms the basis of a correlation relating shaft friction of a driven pile with q_t in clay. The equation, which emerged through calibration against a database of static load tests in clay using Equation (21) as a basis, is provided in Table 2. This is much simpler than Equation (21) due to both compensating factors and limited information in the database.

6.3. Lateral response of piles in sand

A relationship between cone resistance and the horizontal stress developed on laterally loaded piles might be expected given that both CPT and pile involve imposition of lateral strains to the ground. The form of this relationship is, however, unclear.

Suryasentana & Lehane (2014) addressed this uncertainty by conducting 3D Finite Element analyses for laterally loaded piles in a wide variety of sand deposits and, in parallel, performing cavity expansion

analyses to estimate the cone resistances from evaluated limit pressures. A non-linear elasto-plastic constitutive model was employed to model the sand. This model, which is referred to as the Hardening Soil (*HS*) model, is described by Schanz *et. al.* (1999). Initial analyses involved prediction of the cone resistance profile at a site in Mustang Island (Texas) and prediction of the response of a laterally loaded pile at this site (Reese et al. 1974). These analyses, which assumed wished-in-place conditions, showed that the same set of *HS* parameters lead to good predictions for the q_c profile and for the pile's load-displacement response and associated bending moments.

Having verified the suitability of the HS model for prediction of CPT resistance and pile lateral response at Mustang Island, many numerical experiments were conducted involving piles with a range of diameters in sands with fixed relative densities and appropriate *HS* parameters. The sand for each analysis was assumed to have a constant relative density with a CPT resistance determined using the cavity expansion approach at different depths (stress levels). Each analysis predicted pile bending moment (M) and lateral displacement (y) profiles for different levels of lateral load applied at ground level. The net pressures (*P*) were derived by double differentiation of the computed bending moments. Regression analyses were then performed for the full set of *P*, *y* and q_c data computed for piles of various pile diameters (D) at specific depths (z) and vertical effective stresses (σ'_v). The following best-fit relationship emerged:

$$\frac{P}{\sigma'_v D} = 4.2 \left(\frac{q_c}{\sigma'_v}\right)^{0.68} \left(\frac{y}{D}\right)^{0.56} \qquad (22)$$

Equation (22) implies that the net pressure (P) varies with the cone resistance raised to the power of 0.68 and the lateral pile displacement raised to the power of 0.56. These exponents are remarkably similar to those deduced by Novello (1999) and Dyson & Randolph (2001) from physical experiments alone, hence providing support to the numerical approach employed. Suryasentana & Lehane (2016) extended the scope of the 2014 study to a wider range of conditions and proposed the updated formulation provided in Table 3.

7. Effects of cone resistance variability

Variability in CPT profiles at a given site clearly impacts on the foundation response calculated using direct CPT methods. This variability can reflect changes in soil consistency or drainage conditions around a cone, as described below. More rigorous mathematical quantification of the site variability is discussed by Salgado et al. (2019).

7.1. Randomly generated CPT profile

He (2023) examined the effect of CPT variability on capacities calculated for driven piles using the formulations for the Unified method (Table 2) in a variety of single-soil and multi-soil profiles comprising sand, silt and clay. The analyses generated many random q_t and F_r profiles using profiles measured at a number of sites as the basis. Vertical scales of fluctuation, as discussed by Phoon & Kulhawy (1999), of 1m and 2m were employed coupled with coefficients of variation (CoVs) of 0.2 and 0.4.

The predictions showed that, even with a CoV value of 0.4, the variation in calculated shaft capacities was less than 10% and, as expected, reduced with increasing pile length. Calculated end bearing capacities were more sensitive to variability in cone resistance and varied with the assumed vertical scale of fluctuation. The study concluded that that the mean q_c value over the relevant length of the foundation (e.g. pile length for determination of shaft capacity) is the dominant factor affecting the calculated capacity and hence the impact of site variability on pile performance.

7.2. Variable CPT profiles in the field

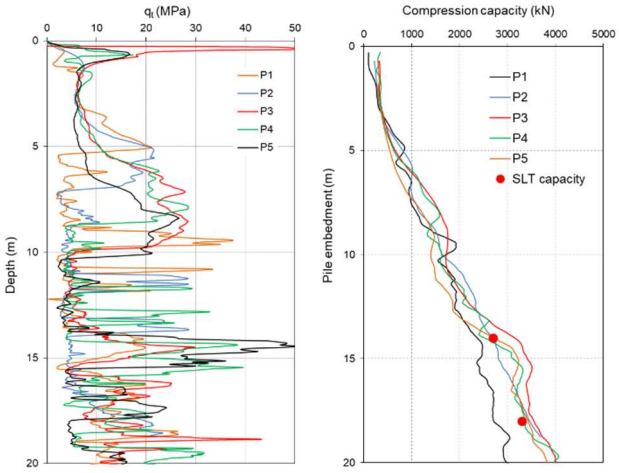

Figure 17 (a) Cone resistances recorded at Perth site and (b) Pile axial capacities calculated for CFA piles using Doan & Lehane (2021) compared with measured capacities in static load tests.

An example of apparent insensitivity of calculated pile capacities to site variability, as indicated by actual CPT profiles, is illustrated on Figure 17a. These profiles were measured for a project where 450mm diameter continuous flight auger piles (CFA) provided foundations for a five-storey building. The soil stratum in which the piles were installed is an alluvial deposit comprising sand, silt and clay layers with various thicknesses and no apparent systematic spatial variation. Static load tests (SLTs) were conducted on 14m and 18m long piles.

The capacities for pile lengths up to 20m were evaluated using the Doan & Lehane (2021) formulations given in Table 3 and are shown on Figure 17. It is seen on Figure 17b that, despite the wide range in q_t profiles, the capacities calculated using the five CPT profiles available are very similar. The calculated capacities for pile lengths of 14m and 18m are in close agreement with measured capacities in the static load tests (SLTs), which corroborates the applicability of the design method.

The shaft friction on a CFA (or bored) pile can be expected to vary with the in-situ lateral effective stress (σ'_{h0}). The success of the Doan & Lehane (2021)

formulations in predicting the pile capacities at this site (and many other sites) can therefore be attributed to the way the method indirectly corrects for different drainage conditions during cone penetration through use of the soil behaviour type index (I_c). The wide variability in q_t seen on Figure 17a therefore arises due to variations in the in-situ permeability and not to variability in σ'_{h0}.

8. Conclusions

This paper describes recent research developments of the author and co-workers in the areas of site and soil characterization using the CPT and in CPT-based foundation design methods. The main observations are summarised as follows:

1. Improved techniques that deal with scale and shallow penetration effects for cone penetration can reconcile previously unexplained differences between laboratory and field experiments. The findings add confidence to the applicability of laboratory-based investigations employing the CPT.
2. The variation of penetration resistance with increasing velocity in any particular silt or clay horizon up to the velocity at which fully undrained conditions is first reached can be most easily determined in practice by conducting a piezocone dissipation test and an additional penetration test at a rate faster than the standard rate.
3. The reliability of the relationship between relative density and cone resistance in granular soil can be improved considerably with a reasonable estimate of the soil's ultimate (critical state) friction angle.
4. While measured cone resistances in deposits with large grain sizes relative to the cone diameter (gravels) fluctuate significantly, averaged q_c values are representative of the density of the deposit.
5. Cone resistance provides a measure of in-situ stress, stiffness and strength and therefore correlations for foundation design need to be consistent with the relative effect of these parameters. Table 1 provides the basis for the proposed correlations for foundation elements which are summarised in Tables 2 and 3. Associated publications show the increased reliability of these correlations which also benefit from the driller independent and digital nature of the CPT data.

Acknowledgements

The author gratefully acknowledges the contributions of past and present researchers at the University of Western Australia in particular, Izal Arafianto, Ahmad Bagbag, Eduardo Bittar, Le Doan, Lichen Li, Bo Liu, Qingbing Liu, Yishan Tian, Yusuke Suzuki, James Schneider, Pauline Truong and Xiangtao Xu.

Notation

B	width of footing or square piles
D	Pile outer diameter
D_e	D for circular pile; $(4B/\pi)0.5$ for square pile of width, B
D_h	diameter of helix
D_i	internal diameter of a pipe pile
F_r	friction ratio (expressed as a percentage) $=f_s/(q_t-\sigma_{v0})$
f_s	cone sleeve friction
f_t/f_c	tension to compression ratio
h	L – z, where L is pile embedment length and z is the depth)
I_c	consistency index, function of Q_{tn} and F_r; see Robertson (2009)
n	stress exponent for Q_{tn}, function of I_c and σ'_{v0}; see Robertson (2009)
P	net lateral pressure
p_a	atmospheric pressure (=100 kPa)
P_u	ultimate net lateral pressure
q	bearing pressure
Q	pile head load
Q_{base}	base capacity
$q_{b0.1}$	base stress at displacement of 10% of diameter
q_{cs}	Average cone resistance along shaft
Q_{shaft}	Shaft capacity
q_t	total (corrected) CPT end resistance (=q_c in sands)
$q_{t,avg}$	average cone resistance within one foundation width (=$q_{c,avg}$ in sands)
Q_{tn}	normalised cone resistance $[(q_t-\sigma_{v0})/p_a]/(p_a/\sigma'_{vo})^n$
SBT	soil behaviour type; see Robertson (2009)
t	pile wall thickness
T	torque
u_g	Pore pressure at ground level
w	vertical displacement (of pile)
w_b	vertical displacement of pile base
y	lateral displacement
δ	pile head vertical displacement
σ_{v0}	total vertical stress
σ'_{v0}	effective vertical stress
τ_f	ultimate shaft friction

References

Andersen, K. H. and Stenhamer, P., 1982. "Static Plate Loading Tests on Overconsolidated Clay." *Journal of the Geotechnical Engineering Division,* 108(GT7), pp. 918-934.

API. ANSI/API RP 2GEO, 2011 "Geotechnical and Foundation Design Considerations". ISO 19901-4:2003 (Modified), Petroleum and natural gas industries-Specific requirements for offshore structures, Part 4-Geotechnical and foundation design considerations. 1st edition. Washington, DC: API Publishing Services.

Bagbag A., Lehane B.M. and Doherty J. 2019. "Non-linear elastic settlement prediction approaches for footings on reconstituted sand" *Canadian Geotechnical Journal*, 56(3), 449-459. https://doi.org/10.1139/cgj-2017-0574

Brand E. W., Muktabhant C. and Taechathummarak A., 1972. "*Load Tests on Small Foundations in Soft Clay".* New York, ASCE, pp. 903-928.

Baldi, G., Bellotti, R. & Ghionna, V., 1986. "Interpretation of CPTs and CPTUs, Part II: Drained Penetration in Sands". *Proc. of 4th International Geotechnical Seminar on Field Instrumentation and In Situ Measurements*, Singapore. https://www.issmge.org/publications/online-library

Bolton, M.D., Gui, M.W., Garnier, J., Corte, J.F., Bagge, G., Laue, J. & Renzi, R., 1999. "Centrifuge cone penetration tests in sand" *Géotechnique*, 49(4), 543-552. https://doi.org/10.1680/geot.1999.49.4.543

Boulanger, R.W.W., and DeJong, J.T.T. 2018. "Inverse filtering procedure to correct cone penetration data for thin-layer and transition effects." *Proc. 4th Int Symp. on Cone Penetration Testing (CPT'18)*, 21-22 June, 2018, Delft, The Netherlands, 25-44. https://doi.org/10.1201/9780429505980

Bittar E., Lehane B.M., Blake A., Richards D., White D., Mahdavi S., and Cerfontaine B. 2023. "CPT based design method for helical piles in sand" *Canadian Geotechnical J.*, https://doi.org/10.1139/cgj-2022-0209.

Briaud, J.-L., and Gibbens, R.M. 1999. "Behavior of five large spread footings in sand." *J. Geotech. Geoenviron. Eng.*, 125(9), 787-796. https://doi.org/10.1061/(ASCE)1090-0241(1999)

Briaud, J-L, and Tucker L.M. 1988. "Measured and predicted axial response of 98 piles." J. *Geotech. Eng. Div*., ASCE, 114(9), 984-1001. https://doi.org/10.1061/(ASCE)0733-9410(1988)114:9(984)

Cerfontaine, B., Brown, M.J., Knappett, J.A., Davidson, C., Sharif, Y.U., Huisman, M., et al. 2021. "Control of screw pile installation to optimise performance for offshore energy applications" *Géotechnique*, 73(3), 234-249. https://doi.org/10.1680/jgeot.21.00118

Doan, L. V. and Lehane, B. M. 2020. "Relating shaft friction of buried piles and CPT resistance in clayey sands." *Géotechnique,* 70(9), 791-802. https://doi.org/10.1680/jgeot.18.P.290

Doan, L. and Lehane, B.M. 2021. "CPT-Based Design Method for Axial Capacities of Drilled Shafts and Auger Cast-in-Place Piles" *J. Geotech. Geoenv. Engineering*, ASCE, 147(8), 1-15. https://doi.org/10.1061/(ASCE)GT.1943-5606.0002542

Dyson, G. J. & Randolph, M. F. 2001. "Monotonic Lateral Loading of Piles in Calcareous Sand." *Journal of Geotechnical and Geoenvironmental Engineering* 127(4) 346–352. https://doi.org/10.1061/(ASCE)1090-0241

Finnie IMS, Randolph MF. 1994. "Punch-through and liquefaction induced failure of shallow foundations on calcareous sediments". Proc. 17th International Conference on the Behaviour of Offshore Structures (BOSS '94), Pergamon Press, 217–230.

Govoni L., Gournevec S. and Gottardi G. (2010). "Centrifuge modelling of circular shallow foundations on sand". Int. J. Phys. modelling Geotechnics, 10(2), 35-46, 35-46. http://doi.org/10.1680/ijpmg.2010.10.2.35.

Houlsby, G.T. & Hitchman, R., (1988). "Calibration chamber tests of a cone penetrometer in sand". Geotechnique, 38(1), 39-44. https://doi.org/10.1680/geot.1988.38.1.39

Jardine, R. J., Chow, F. C., Overy, R. & Standing, J. R. 2005. "*ICP design methods for driven piles in sands and clays."* Thomas Telford. https://www.icevirtuallibrary.com/doi/abs/10.1680/

Jaeger, R. A., DeJong, J. T., Boulanger, R. W., Low, H. E. & Randolph, M. F. (2010). Variable penetration rate CPT in an intermediate soil. 2nd Int. Symp. on Cone Penetration Testing, Huntington Beach, US.http://www.cpt10.com

Jamiolkowski, M., Lo Presti, D.C.F. and Manassero, M., 2003. "Evaluation of relative density and shear strength of sands from CPT and DMT." In *soil behavior and soft ground construction*. 201-238. https://doi.org/10.1061/40659(2003)7

Kim, K., Prezzi, M., Salgado, R. & Lee, W. 2008 "Effect of penetration rate on cone penetration resistance in saturated clayey soils" J. Geotech. and Geoenv. Engng, 134(8),1142-1153.https://doi.org/10.1061/(ASCE)1090-0241(2008)

Govoni, L., Gournevec, S. and Gottardi, G. 2010. "Centrifuge modelling of circular shallow foundations on sand." Int. J. Physical modelling in Geotechnics, 10(2), 35-46, http://doi.org/10.1680/ijpmg.2010.10.2.35.

He, J. 2023. "Assessment of effects of cone resistance variability on predictions of axial capacity." Final year dissertation, University of Western Australia.

Jamiolkowski, M., D. C. Lo Presti, and M. Manassero. "Evaluation of Relative Density and Shear Strength of Sands from CPT and DMT." In Geotechnical Special Publication, 119:201–38. New York, NY: American Society of Civil Engineers, 2003. https://doi.org/10.1061/40659(2003)7

Jardine, R. J., Lehane, B. M., Smith, P. R. and Gildea, P. A. 1995. "Vertical loading experiments on rigid pad foundations at Bothkennar". *Geotechnique* 45(4), 573-597, https://doi.org/10.1680/geot.1995.45.4.573

Lehane, B.M. 2003. "Vertically loaded shallow foundation on soft clayey silt: A case history." *Geotechnical Engineering, ICE*, 156, 17-26. https://doi.org/10.1680/geng.2003.156.1.17

Lehane B.M. 2012. "Foundation capacity from the CPT". *Proc. 4th Int. Conf. on Geotechnical and Geophysical Site Characterisation,* 1, ISC4, Recife, Brazil, 63-82. https://www.crcpress.com/Geotechnical-and-Geophysical-Site-Characterization-4/Coutinho-Mayne/9780415621366

Lehane B.M., Doherty J.P. and Schneider J.A. 2009. "Settlement prediction for footings on sand.", *Proc. 4th Int. Symp. on deformation characteristics of Geomaterials*, Atlanta, 1, 133-152, IOS press, The Netherlands. https://www.issmge.org/publications/online-library

Lehane, B.M., Bittar, E., Lacasse, S., Liu, Z. and Nadim, F. 2022. "New CPT methods for evaluation of the axial capacity of driven piles." *Proc. 5th Int. Symp. On Penetration Testing*, CPT22, Bologna. Gottardi, G. & Tonni, L. (eds.). CRC Press, p. 3-15. http://doi.org/10.1201/9781003308829-1

Lehane B.M., Liu Z,. Bittar E., Nadim F., Lacasse S., Jardine R.J., Carotenuto P., Jeanjean P., Rattley M., Gavin K., Gilbert R., Haavik J. and Morgan N. 2020. "A new CPT-based axial pile capacity design method for driven piles in sand." *Proc 4th Int. Symposium on Frontiers in Offshore Geotechnics*, ISFOG-4, Texas, 463-47 https://www.isfog2020.org/proceedings

Lehane, B., Li, L. and Bittar, E. 2020. "CPT-based load-transfer formulations for driven piles in sand." *Geotechnique Letters*, 10, 568-574. http://doi.org/10.1680/jgele.20.00096

Lehane B.M., Ismail M. and Fahey M. 2004. "Seasonal dependence of in-situ test parameters in sand above the water table." *Geotechnique*, 54 (3), 215-218. https://doi.org/10.1680/geot.2004.54.3.215

Lehane, B.M., Zania, V., Chow, S.H. & Jensen, M. 2023. "Interpretation of centrifuge CPT data in normally consolidated silica and carbonate sands." Geotechnique, 73(10, 907-916, https://doi.org/10.1680/jgeot.21.00177

Liu B., Xue J., Lehane B.M. and Yin, Z. 2023. "An improved creep correction factor for the settlement of shallow foundations on sand based on macro element simulations". ICE, Geotechnical Engineering, http://dx.doi.org/10.1680/jgeen.23.00049

Liu, Q. and Lehane B.M.. 2012. "The influence of particle shape on the Cone Penetration Test (CPT) end resistance in uniformly graded granular soils." *Geotechnique*, 62(11), 973-984. https://doi.org/10.1680/geot.10.P.077

Liu, Q. and Lehane, B.M. 2021. "A centrifuge investigation of the relationship between the vertical response of footings on sand and CPT end resistance." *Geotechnique* 71(5), 455-465 *https://doi.org/10.1680/jgeot.19.P.253*

Liu, Q. and Lehane B.M.. 2012. "The influence of particle shape on the Cone Penetration Test (CPT) end resistance in uniformly graded granular soils." *Geotechnique*, 62(11), 973-984. https://doi.org/10.1680/geot.10.P.077

Liu B., Lehane, B.M. and Xue J. 2022. "A one-dimensional elasto-viscoplastic macro-element model for creep analysis of shallow foundations on sand". *Computers & Geotechnics*,142 https://doi.org/10.1016/j.compgeo.2021.104561

Lunne, T. & Christoffersen, H.P., 1983 "Interpretation of cone penetrometer data for offshore sands". In Offshore Technology Conference. OTC-4464-MS., https://doi.org/10.4043/4464-MS

Mayne, P. W. 2014. "Interpretation of geotechnical parameters from seismic piezocone tests." *Proc. 3rd Int. Symp. On Cone Penetration Testing, CPT14*, Las Vegas, USA, 1, 47-73. http://www.cpt14.com

Novello, E. A. 1999. "From static to cyclic p-y data in calcareous sediments." *Engineering for calcareous sediments* **1**, 17–24. https://doi.org/10.1201/9781003211433

Phoon, K.K. and Kulhawy, F.H 1999. "Characterization of geotechnical reliability". *Canadian Geotechnical J.*, 36, 612-624. https://doi.org/10.1139/t99-038

Pucker, T., Bienen, B., & Henke, S. 2013. "CPT based prediction of foundation penetration in siliceous sand." Applied Ocean Research, 41, 9-18. https://doi.org/10.1016/j.apor.2013.01.005.

Rogers J.D. 2006. "Subsurface exploration using the Standard Penetration Test and Cone Penetrometer Test." *Environmental & Engineering Geoscience*, 12(2), 161-179. http://dx.doi.org/10.2113/12.2.161

Reese, L. C., Cox, W. R. & Koop, F. D. 1974. "Analysis of laterally loaded piles in sand." *6th Offshore Technology Conference, Houston, Texas.* https://doi.org/10.4043/2080-MS

Robertson, P.K. (2009). Interpretation of cone penetration tests - A unified approach. *Canadian Geotechnical J.*, 46(11):1337-1355. https://doi.org/10.1139/T09-065.

Salgado R., Ganju E. and Prezzi M. (2019). Site variability analysis using cone penetration test data. Computers and Geotechnics, 105, 37-50. https://doi.org/10.1016/j.compgeo.2018.08.001

Salgado R., Mitchell J.K. and Jamiolkowski M. 1997. "Cavity expansion and penetration resistance in sand." *J. Geotech Geoenv Engineering, ASCE, 123 (4)*. https://doi.org/10.1061/(ASCE)1090-0241(1997)123:4(344)

Schanz, T., Vermeer, P. A. & Bonnier, P. G. 1999. "The hardening soil model: formulation and verification." In *Beyond 2000 in computational geotechnics: 10 Years of Plaxis*, 1–16. https://doi.org/10.1201/9781315138206

Schneider„J.A. and Lehane, B.M. 2006. "Effects of width for square centrifuge displacement piles in sand." *Proc. 6th Int. Conf. Physical Modelling in Geotechnics*, Hong Kong ed., Vol. 2, 867-873.

Silva M.F. 2005. Numerical and physical models of rate effects in soil penetration. PhD Thesis, Univ. of Cambridge, UK.

Sreng, S., Ueno, K., Mochizuki, A., & Ma, X. 2005. "Image analysis of shallow foundation tests on sand ground and their FE-analysis using a new elasto-plastic model." *Proc. of the 16th ICSMGE*, A.A Balkema Publishers, Vol. 16, No. 2, 985-998. https://www.issmge.org/publications/online-library

Suryasentana S. and Lehane B.M. 2014. "Numerical derivation of CPT-based *p-y* curves for piles in sand." *Geotechnique*, 64(3), 186-194. https://doi.org/10.1680/geot.13.P.026

Suryasentana, S. and Lehane, B.M. 2016. "Updated CPT-based p-y formulation for laterally loaded piles in cohesionless soil under static loading." *Geotechnique*, 66(6), 445-453. http://doi.org/10.1680/jgeot.14.P.156

Suzuki, Y. 2014. "Investigation and interpretation of cone penetration rate effects." PhD Thesis, University of Western Australia.

Suzuki, Y. and Lehane, B.M. 2015. "Cone Penetration at variable penetration rates in kaolin-sand mixtures." *Int. J. Physical Modelling in Geotechnics*, 15(4), 209-219. https://doi.org/10.1680/ijpmg.14.00043

Teh, C. I. & Houlsby, G. T. 1991. "An analytical study of the cone penetration test in clay". Géotechnique, 41, No. 1, 17-34. https://doi.org/10.1680/geot.1991.41.1.17

Tian Y. and Lehane B.M. 2022. **"**Parameters affecting the CPT resistance of reconstituted sands." *Proc. 5th Int. Symp. on Cone Penetration Testing, CPT 2022.* Gottardi, G. & Tonni, L. (eds.). CRC Press, 1, 734-740. https://www.taylorfrancis.com/chapters/oa-edit/10.1201

Tian, Y. and Lehane, B.M. 2024a. "The influence of soil layering on cone penetration resistance". (submitted to *Geotechnique*).

Tian, Y. and Lehane, B.M. 2024b. "Investigation of the relationship between CPT cone resistance and friction angle for a range of granular soils". *Proc. 7th International Conference on Geotechnical and Geophysical Site Characterization*, Barcelona, 18 - 21 June 2024.

Tian, Y. and Lehane, B.M. 2024c. "An investigation of relationships between relative density and cone resistance in granular deposits." (submitted to Int. J. Physical Modelling in Geotechnics).

Truong P. and Lehane B.M. 2018. "Effects of pile shape and pile end configuration on the lateral response of displacement piles in soft clay". *Geotechnique*, 68(9), 794-804. https://doi.org/10.1680/jgeot.16.P.291 .

Yu, H. S. & Carter, J. P. 2002. "Rigorous Similarity Solutions for Cavity Expansion in Cohesive-Frictional Soils." *International Journal of Geomechanics*, 2(2), 233-258. https://doi.org/10.1080/15323640208500181

Yu, H. S. & Mitchell, J. K. 1998. "Analysis of Cone Resistance: Review of Methods." *Journal of Geotechnical and Geoenvironmental Engineering*, 124(2), 140-149. https://doi.org/10.1061/(ASCE)1090-0241(1998)124:2(140)

Xu, X. (2007). Investigation of the end bearing performance of displacement piles in sand. PhD Thesis. University of Western Australia.